



## Article

# Comparison of GPM IMERG Version 06 Final Run Products and Its Latest Version 07 Precipitation Products across Scales: Similarities, Differences and Improvements

Yaji Wang <sup>1,2</sup>, Zhi Li <sup>3</sup> , Lei Gao <sup>1,\*</sup>, Yong Zhong <sup>4</sup> and Xinhua Peng <sup>1,2</sup>

- <sup>1</sup> State Key Laboratory of Soil and Sustainable Agriculture, Institute of Soil Science, Chinese Academy of Sciences, Nanjing 210008, China; wangyaji@issas.ac.cn (Y.W.)
- <sup>2</sup> University of Chinese Academy of Sciences, Beijing 100081, China
- <sup>3</sup> Department of Earth System Science, Stanford University, Stanford, CA 94025, USA
- <sup>4</sup> Collaborative Innovation Center for Water Pollution Control and Water Safety in Karst Areas, Guilin University of Technology, Guilin 541004, China
- \* Correspondence: lgao@issas.ac.cn

**Abstract:** Precipitation is an essential element in earth system research, which greatly benefits from the emergence of Satellite Precipitation Products (SPPs). Therefore, assessment of the accuracy of the SPPs is necessary both scientifically and practically. The Integrated Multi-Satellite Retrievals for GPM (IMERG) is one of the most widely used SPPs in the scientific community. However, there is a lack of comprehensive evaluation for the performance of the newly released IMERG Version 07, which is essential for determining its effectiveness and reliability in precipitation estimation. In this study, we compare the IMERG V07 Final Run (V07\_FR) with its predecessor IMERG V06\_FR across scales from January 2016 to December 2020 over the globe (cross-compare their similarities and differences) and a focused study on mainland China (validate against 2481 rain gauges). The results show that: (1) Globally, the annual mean precipitation of V07\_FR increases 2.2% compared to V06\_FR over land but decreases 5.8% over the ocean. The two SPPs further exhibit great differences as indicated by the Critical Success Index (CSI = 0.64) and the Root Mean Squared Difference (RMSD = 3.42 mm/day) as compared to V06\_FR to V07\_FR. (2) Over mainland China, V06\_FR and V07\_FR detect comparable precipitation annually. However, the Probability of Detection (POD) improves by 5.0%, and the RMSD decreases by 3.7% when analyzed by grid cells. Further, the POD (+0%~+6.1%) and CSI (+0%~+8.8%) increase and the RMSD (−11.1%~0%) decreases regardless of the sub-regions. (3) Under extreme rainfall rates, V07\_FR measures 4.5% lower extreme rainfall rates than V06\_FR across mainland China. But V07\_FR tends to detect more accurate extreme precipitation at both daily and event scales. These results can be of value for further SPP development, application in climatological and hydrological modeling, and risk analysis.



**Citation:** Wang, Y.; Li, Z.; Gao, L.; Zhong, Y.; Peng, X. Comparison of GPM IMERG Version 06 Final Run Products and Its Latest Version 07 Precipitation Products across Scales: Similarities, Differences and Improvements. *Remote Sens.* **2023**, *15*, 5622. <https://doi.org/10.3390/rs15235622>

Academic Editor: Kenji Nakamura

Received: 7 November 2023

Revised: 29 November 2023

Accepted: 1 December 2023

Published: 4 December 2023



**Copyright:** © 2023 by the authors. Licensee MDPI, Basel, Switzerland. This article is an open access article distributed under the terms and conditions of the Creative Commons Attribution (CC BY) license (<https://creativecommons.org/licenses/by/4.0/>).

**Keywords:** satellite; precipitation; GPM; IMERG; extremes

## 1. Introduction

Precipitation is the key driver of the Earth's hydrological system, which can substantially affect societies and ecosystems [1]. Specifically, precipitation is a pivotal element in climate modeling, natural disaster emergency responses, and water resource management [2–5]. Therefore, the precise estimates of precipitation across scales hold great promise to improve scientific understanding and better risk management. Generally, three primary techniques are used for precipitation measurement: ground gauges, weather radars, and satellite-based remote sensing [6]. Satellite Precipitation Products (SPPs) harness data acquired from various sources, including the geosynchronous-Earth-orbit infrared instruments, passive microwave (PMW) sensors, and spaceborne radars onboard low-Earth-orbiting satellites [5]. SPPs exhibit advantages over the other two types of measurements

in large-scale applications due to their wide coverage and unprohibited views and are now widely used in areas such as hydrology, climate change, and agriculture [7,8].

There are two consecutive satellite precipitation missions for global precipitation monitoring. The National Aeronautics and Space Administration (NASA) and the Japan Aerospace Exploration Agency (JAXA) first initiated the Tropical Rainfall Measuring Mission (TRMM) satellite in 1997. The TRMM was launched to thoroughly explore the evolution of tropical precipitation aided by the first spaceborne precipitation radar (PR) and microwave imager (MI). As the successor of TRMM, the Global Precipitation Measurement (GPM) mission started in February 2014 and covers a greater extent (i.e., 65°N-S). The GPM Core Observatory (GPM CO) also demonstrates superior capabilities over the TRMM in monitoring instruments, carrying the Dual-Frequency Precipitation Radar (DPR) and the multichannel GPM Microwave Imager (GMI). Equipped with advanced monitoring devices, the GPM CO is capable of extending the measurement scope of precipitation, including light rainfall and falling snow [9]. With these precipitation monitoring missions, numerous quasi-global SPPs have been developed [10–12]. Of all the SPPs, the level-3 product Integrated Multi-Satellite Retrievals for GPM (IMERG, [13]) released by NASA has gained widespread interest within the hydrological community [14]. Each IMERG version comes with three runs, namely the Early Run (ER), Late Run (LR), and Final Run (FR), with different latencies to accommodate user needs. The IMERG system has been updated five times since its inception, starting with the IMERG V03 to the latest IMERG V07, which was released in July 2023.

Among all the versions of IMERG, the IMERG V06 has gained substantial attention in the current scientific community due to its superiority over former versions. Evaluations of IMERG V06 span global and regional scales. Globally, Li et al. [15] conducted a comprehensive 20-year comparison of V06\_ER and V06\_FR, revealing distinct application scenarios for each product. Regionally, Hamza et al. [16] assessed V06\_FR, along with three other SPPs, at varying temporal resolutions in a mountainous area of Pakistan. Similar regional assessments were conducted by Moazami and Najafi [17] in Canada and Yu et al. [18] in China. Beyond overall precipitation rates, precipitation at specific rates has also been evaluated. For example, Li et al. [19] analyzed the capability of V06\_FR in detecting light rainfall and identified the potential error sources. With regard to extreme precipitation events and recognizing their significant social and economic implications, the performance of V06 products under extreme precipitation rates has undergone extensive evaluation, such as by Zhou et al. [20] over Hubei province, China, and Aksu et al. [21] over Türkiye. With the increasing expansion of validation efforts, the application of IMERG V06 has emerged in various fields, especially FR, due to its accuracy through calibration. For example, Ang et al. [22] demonstrated the superiority of V06\_FR in simulating streamflow and evaporation in Southeast Asia compared with a series of re-analysis products and SPPs. Ham et al. [1] detected the trend of climate change employing IMERG as one of the precipitation datasets. What is more, numerous related studies, including catchment modeling and environmental pollution, have been carried out in different regions of China due to a lack of high spatial–temporal forcing data or the urgent need for future risk mitigation [23–25].

Despite its current widespread use, certain limitations still exist in IMERG V06, such as the potential orographic effects on the motion vectors and the risk of introducing artifacts in the propagated estimates in high-latitude regions [26]. The IMERG V07\_FR has been continuously released since July 2023, and data were processed in retrospect ranging from January 2000 to May 2023. There are several upgrades of the newly released version 07, i.e., updating the IR quality assurance and the IR precipitation algorithm and assessing the applicability of the Goddard Profiling Algorithm Microwave (GPROF MW) estimates over snowy surfaces [27]. Some existing deficiencies of IMERG V06 have been addressed in the V07 product to improve the level of global precipitation measurement [28]. However, to the best of our knowledge, a thorough assessment of IMERG V07\_FR with its predecessor, IMERG V06\_FR, is still lacking either at the global scale or the regional scale. This study

provides an early assessment of IMERG V07 as compared to V06 on a global scale and is also validated against rain gauges in mainland China. Notably, in addition to evaluating the entire product, an extra assessment is also conducted specifically for extreme precipitation to consider its practical implications.

Therefore, we compare the performance of IMERG V06\_FR and V07\_FR across scales since the start of GPM era. The objectives of this study are: (1) investigating the differences between IMERG V06\_FR and V07\_FR products over the globe at  $0.1^\circ \times 0.1^\circ$  spatial and daily temporal resolution; (2) evaluating and comparing IMERG V06\_FR and V07\_FR over mainland China against ground-based observations; (3) assessing the performance of these two products under extreme precipitation rates on the regional basis. This paper is organized as follows: Section 2 introduces the study region, datasets, and statistical methods. Section 3 compares IMERG V06\_FR and V07\_FR at the global, national, and regional scales. Section 4 discusses the reasons for the similarities and differences between the upgraded V07\_FR and its predecessor V06\_FR. Section 5 concludes the study and proposes potential suggestions for future work.

## 2. Materials and Methods

### 2.1. Study Area

Global precipitation covers  $90^\circ\text{N-S}$  at a daily time interval, considering the improvements of IMERG V06 and V07 in data coverage [15]. As for nationally based analysis, the mainland China was chosen as a study focus (Figure 1a). Eight sub-regions were further divided by distinct climatic characteristics, as shown in Figure 1b, namely the western arid and semi-arid (WAS) region, the Qinghai-Tibet (QT) region, the eastern arid (EA) region, and the southern (S), central (C), northern (N), northeastern (NE), and southwestern (SW) region of mainland China [29,30]. The regional analysis was conducted according to the sub-region division to further investigate the performance of different versions of satellite products. To completely assess the precipitation products, the southeast coastline area of mainland China (Figure 1c) was chosen as the target area to evaluate the precipitation estimation during typical typhoon events. The selected southeast coastline area can be referred to Sui et al. [31], and this area tends to be attacked by typhoon events, such as Meranti (2016) and Khanun (2017).

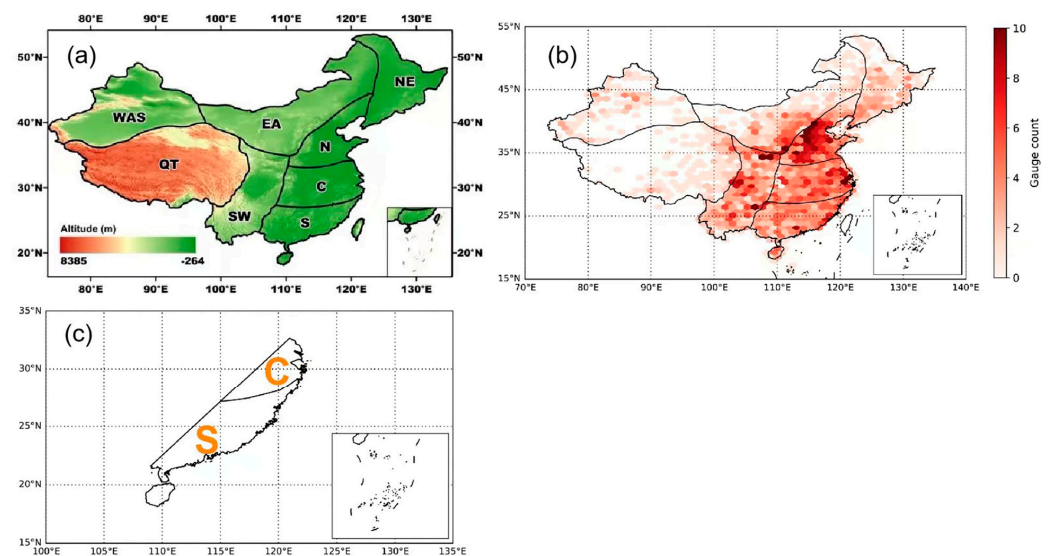


**Figure 1.** The eight climatic sub–regions across China (a), the ground gauge distribution (b), and the southeast coastline area of mainland China (c). Partly cited from Shen et al. [32].

## 2.2. Datasets

### 2.2.1. IMERG

The IMERG precipitation data were used in the current study. The IMERG product integrates various data sources, including satellite-derived microwave precipitation estimates, microwave-calibrated infrared estimates, ground gauge measurements, and other potential datasets, at spatial and temporal resolutions of  $0.1^\circ \times 0.1^\circ$  and half-hourly intervals [33]. This dataset contained three stages with different latencies: early run (ER, 4 h), late run (LR, 12 h), and final run (FR, 3.5 months). ER and LR both provided near-real-time estimates without gauge calibration, while the FR was calibrated using the monthly Global Precipitation Climatology Center dataset (GPCC). The FR is considered to be of high accuracy and designed for scientific research purposes [33]. Therefore, the current mostly used IMERG V06\_FR and the latest IMERG V07\_FR are used for global, national, and event precipitation assessment. The IMERG V06 was initially released in March 2019, over 4 years prior to IMERG V07. It is noteworthy that the V06 product underwent self-upgrades due to data correction, evolving from its original version V06A to V06B in May 2019 [34]. Consequently, all references to IMERG V06 in this study pertain to IMERG V06B. It is also important to mention that all references to IMERG V07 refer to IMERG V07A, as the newly released product has not undergone upgrades.

The data used in the current study span from January 2016 to December 2020, within the range of the GPM era. The IMERG V06\_FR and V07\_FR products can be accessed at [https://disc.gsfc.nasa.gov/datasets/GPM\\_3IMERGDE\\_06/summary?keywords=IMERG](https://disc.gsfc.nasa.gov/datasets/GPM_3IMERGDE_06/summary?keywords=IMERG) (accessed on 14 August 2023) and [https://disc.gsfc.nasa.gov/datasets/GPM\\_3IMERGDF\\_07/summary?keywords=IMERG](https://disc.gsfc.nasa.gov/datasets/GPM_3IMERGDF_07/summary?keywords=IMERG) (accessed on 14 August 2023), respectively.

### 2.2.2. Rain Gauge Dataset

The ground rain gauge dataset was obtained from the National Meteorological Information Center of the China Metrological Administration (CMA). This dataset covered 2481 gauges over mainland China and measured precipitation at daily resolution (Figure 1a). This dataset was independent of the IMERG dataset, so it was chosen as the reference data for evaluating the performance of the target satellite products. The used ground gauge dataset shared the same temporal coverage as the selected IMERG products. Notably, the gauges were organized into  $0.1^\circ \times 0.1^\circ$  grid cells to conform to the IMERG products' spatial resolution. Evaluation was limited to grid cells containing at least one gauge. In cases where a grid cell contained multiple gauges, the average value was used for analysis.

### 2.2.3. Extreme Precipitation Dataset

The dataset, for extreme precipitation was derived from the IMERG and rain gauge datasets over mainland China, adopting the threshold of greater than 50 mm/day, respectively. The extracted datasets were also processed to conform to the  $1^\circ \times 1^\circ$  spatial resolution, as described in Section 2.2.2. At the event scale, 5 typical typhoon events were selected based on their features, including start and end date, duration, and maximum rainfall amount.

### 2.2.4. Earth Surface Data

Considering the different climatic and topographic conditions between lands and oceans, the coastline data were used to investigate the performance of land and ocean areas, respectively. It can be accessed at <https://www.naturalearthdata.com/downloads/10m-physical-vectors/10m-coastline/> (accessed on 7 September 2023).

## 2.3. Statistical Analysis

A list of evaluation metrics, corresponding equations, and the best values is summarized in Table 1, in which IMERG V07\_FR and ground gauge serve as the estimated values for global and national assessment, respectively. The IMERG products were examined from

two perspectives. First, the detectability of SSP was qualitatively evaluated by categorical indices, including the probability of detection (POD), false alert ratio (FAR), and critical successful index (CSI). The analysis employed a widely accepted threshold of 1 mm/day to distinguish between precipitation and non-precipitation events [35,36]. Second, the SSPs' accuracy in precipitation estimation was analyzed quantitatively using continuous indices containing relative bias (RB), mean absolute difference (MAD), root mean squared difference (RMSD), and normalized root mean squared difference (normalized RMSD). The RB and RMSD reflect the systematic and random components of errors. MAD quantified the mean difference between the target SSP and reference data. The normalized RMSD was especially calculated to reduce the error raised by rainfall rates over seas and lands, respectively.

**Table 1.** A list of statistical metrics in evaluation IMERG Final Run with the benchmark product.

	Metrics	Formula	Best Value
Categorical index	Probability of Detection (POD)	$\frac{n_{11}}{n_{11}+n_{01}}$	1
	False Alarm Rate (FAR)	$\frac{n_{10}}{n_{11}+n_{10}}$	0
	Critical Success Index (CSI)	$\frac{n_{11}}{n_{11}+n_{10}+n_{01}}$	1
Continuous index	Relative Bias (RB)	$\frac{\sum_{i=1}^N (FR_i - B_i)}{\sum_{i=1}^N B_i}$	0
	Mean Absolute Difference (MAD)	$\frac{1}{N} \sum_{i=1}^N  FR_i - B_i $	0
	Root mean squared difference (RMSD)	$\sqrt{\frac{1}{N} \sum_{i=1}^N (FR_i - B_i)^2}$	0
	Normalized root mean squared difference (normalized RMSD)	$\frac{\sqrt{\frac{1}{N} \sum_{i=1}^N (FR_i - B_i)^2}}{\overline{FR}}$	0

$FR_i$  refers to the value of selected final run (FR) product, while  $B_i$  refers to the corresponding value of selected benchmark product, i.e., IMERG V07\_FR or gauge value in the present study.  $N$  is the number of samples;  $n_{11}$  refers to the number of precipitation events observed by selected FR product and its benchmark product at the same time;  $n_{10}$  is the number of precipitation events observed by selected FR product not by its benchmark;  $n_{01}$  is the opposite of  $n_{10}$ .

Taylor diagrams [37] were adopted in the current study to assess the performance of IMERG products against the ground gauge. The Taylor diagram was essentially an integration of three statistical metrics, including the correlation coefficient (CC), standard deviation (SD), and RMSD, into a polar plot based on the cosine relationship between them. In the polar plot, both IMERG products and ground gauge data are represented as data points. The proximity of the IMERG point to the ground gauge point is indicative of the product's performance quality. Specifically, the closer the IMERG point is to the ground gauge, the better the performance of the product is. A flowchart with the main research objectives and methodology discussed above is sketched in Figure 2. Notably, results for global analysis are conducted using data from all  $0.1^\circ \times 0.1^\circ$  grid cells unless otherwise specified.

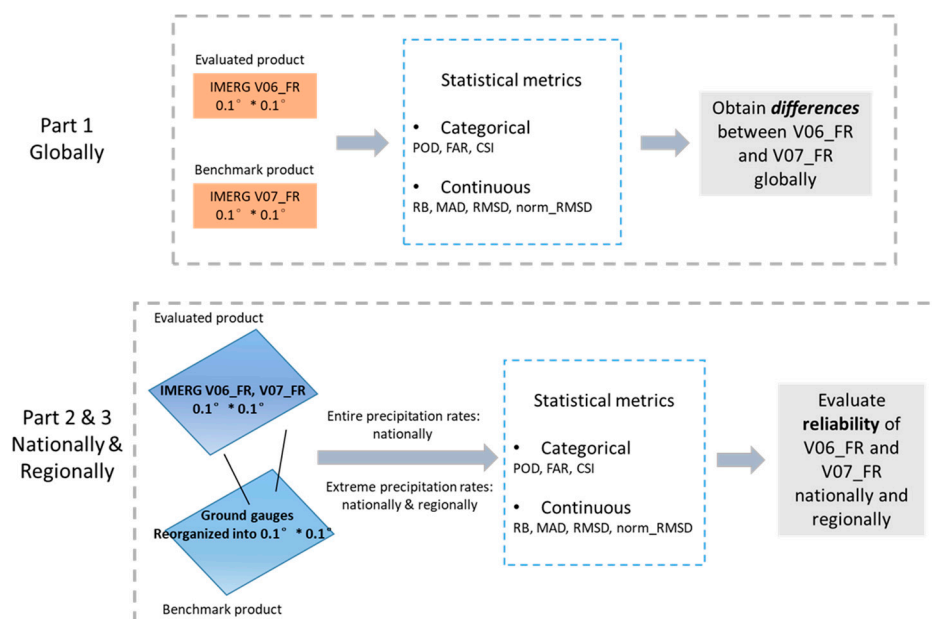


**Figure 2.** Flowchart of IMERG intercomparison across scales.

### 3. Results

#### 3.1. Comparison of IMERG V06\_FR and V07\_FR at Global Scale

##### 3.1.1. Global Analysis of Annual Precipitation Rate

IMERG V07\_FR exhibits differences compared to V06\_FR from January 2016 to December 2020 at a global scale (Figure 3). The mean global annual rainfall for V07\_FR (775.7 mm/year) is slightly lower than that of the V06\_FR (800.1 mm/year), and the spatial distribution of estimated precipitation is comparable as for the two IMERG products. Similar precipitation among different versions of Final Run products is a frequently observed phenomenon, as introduced by Wang et al. [14]. This consistency is primarily attributed to the gauge correction process, which incorporates data from the GPCP dataset. However, the maximum annual mean rainfall for V07\_FR (11,698.8 mm/year) is much greater than that of V06\_FR (9455.0 mm/year), both inside the intertropical convergence zone (ITCZ). The result of zonal maxima aligns with previous findings by Wang et al. [14] and Li et al. [15]. The mean annual rainfall over the ocean tends to be higher than that over land, whatever the SPP version. Further, V07\_FR is higher than V06\_FR over land (487.0 vs. 476.3 mm/year) but has lower annual mean rainfall over the ocean (915.8 vs. 957.2 mm/year). However, both maxima over land and ocean for IMERG V07\_FR were larger than those for IMERG V06\_FR (land: 8295.3 vs. 7403.3 mm/year; ocean: 11,698.8 vs. 9455.0 mm/year), all located near the coastline of Columbia, South America, contingent with the North Pacific Ocean.

The spatial differences between IMERG V07\_FR and V06\_FR are shown in Figure 3c. Although the annual mean difference between these two products is around 30 mm/year, the greatest difference between them is up to 5049.6 mm/year (V06\_FR = 0 mm/year and V07\_FR = 5049.6 mm/year), located in the Lare glacier, Alaska, the USA. This discrepancy is attributed to the detection of precipitation for this region by V07 FR but not by V06 FR. In comparison to V06\_FR, V07\_FR estimates lower precipitation for nearly 60% of the grid cells globally, mainly located within the Antarctic Ocean. It is interesting to observe that IMERG V07\_FR tends to overestimate V06\_FR over the equator. This phenomenon can be attributed to the uncertainties arising from the abundant local precipitation.

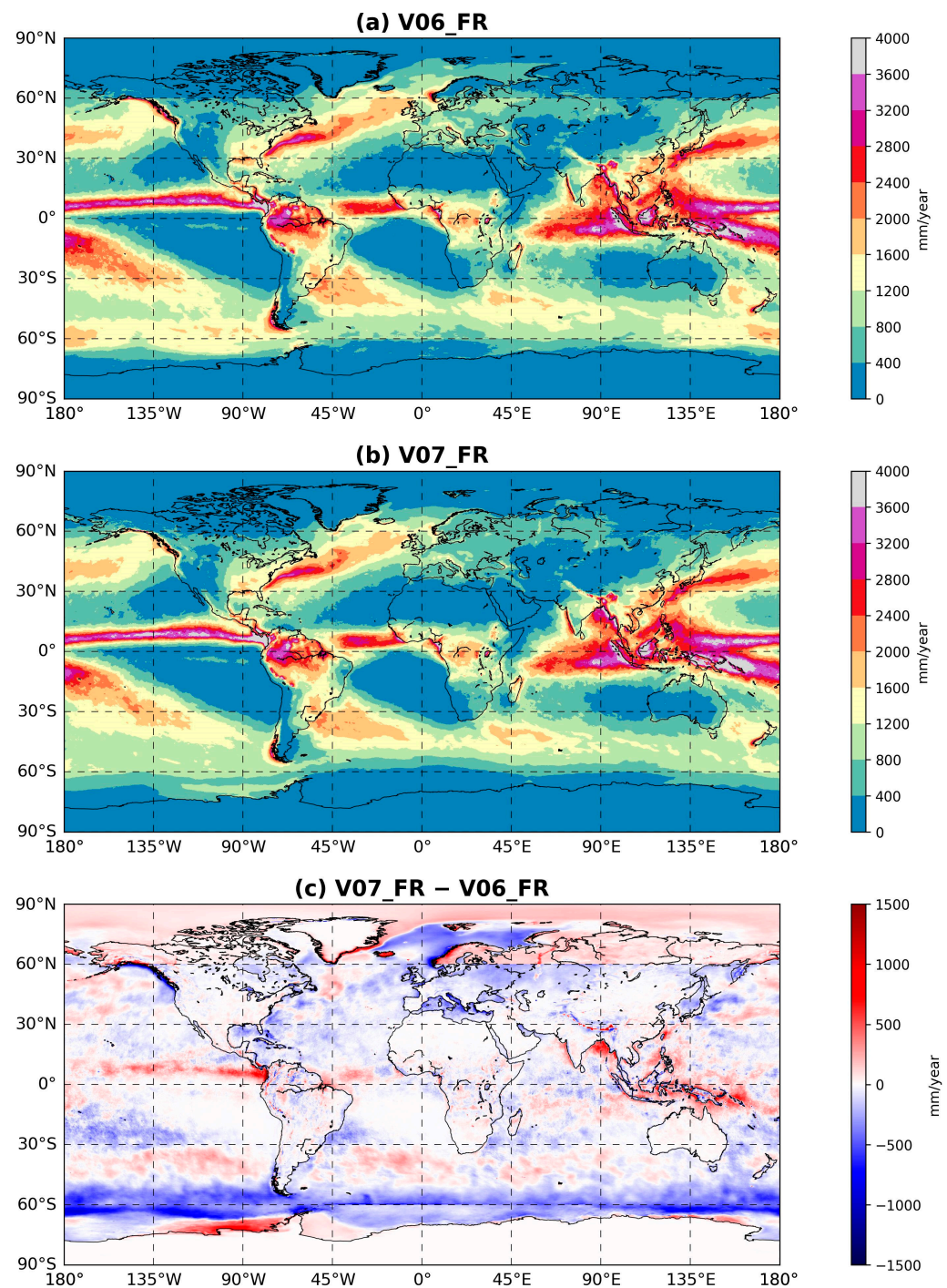


**Figure 3.** Spatial distribution of global annual mean precipitation estimated by IMERG V06\_FR (a), V07\_FR (b), and their differences (c).

### 3.1.2. Statistical Analysis of Daily Precipitation Rate

Figure 4 illustrates the global distribution of the statistical metrics described in Table 1 using the daily precipitation dataset. Figure 4a–c provides the categorical index distribution of precipitation revealed by IMERG V06\_FR compared with V07\_FR. The values of POD, FAR, and CSI indicate both V06\_FR and V07\_FR are capable of successfully detecting precipitation globally. However, these three metrics indicate disparities in precipitation detection among IMERG versions (0.79, 0.24, and 0.64). The differences are still evident for dry regions (characterized by mean annual rainfall below 500 mm), specifically in areas such as the Pacific Ocean close to the western coast of South America and the Atlantic

Ocean close to the western coast of South Africa, where the POD falls below 0.5, and the FAR exceeds 0.6. The categorical indexes over lands and ocean surfaces exhibit a similar level, with slightly better performance over lands than over oceans (POD: 0.80 vs. 0.79, FAR: 0.23 vs. 0.24, and CSI: 0.65 vs. 0.63).

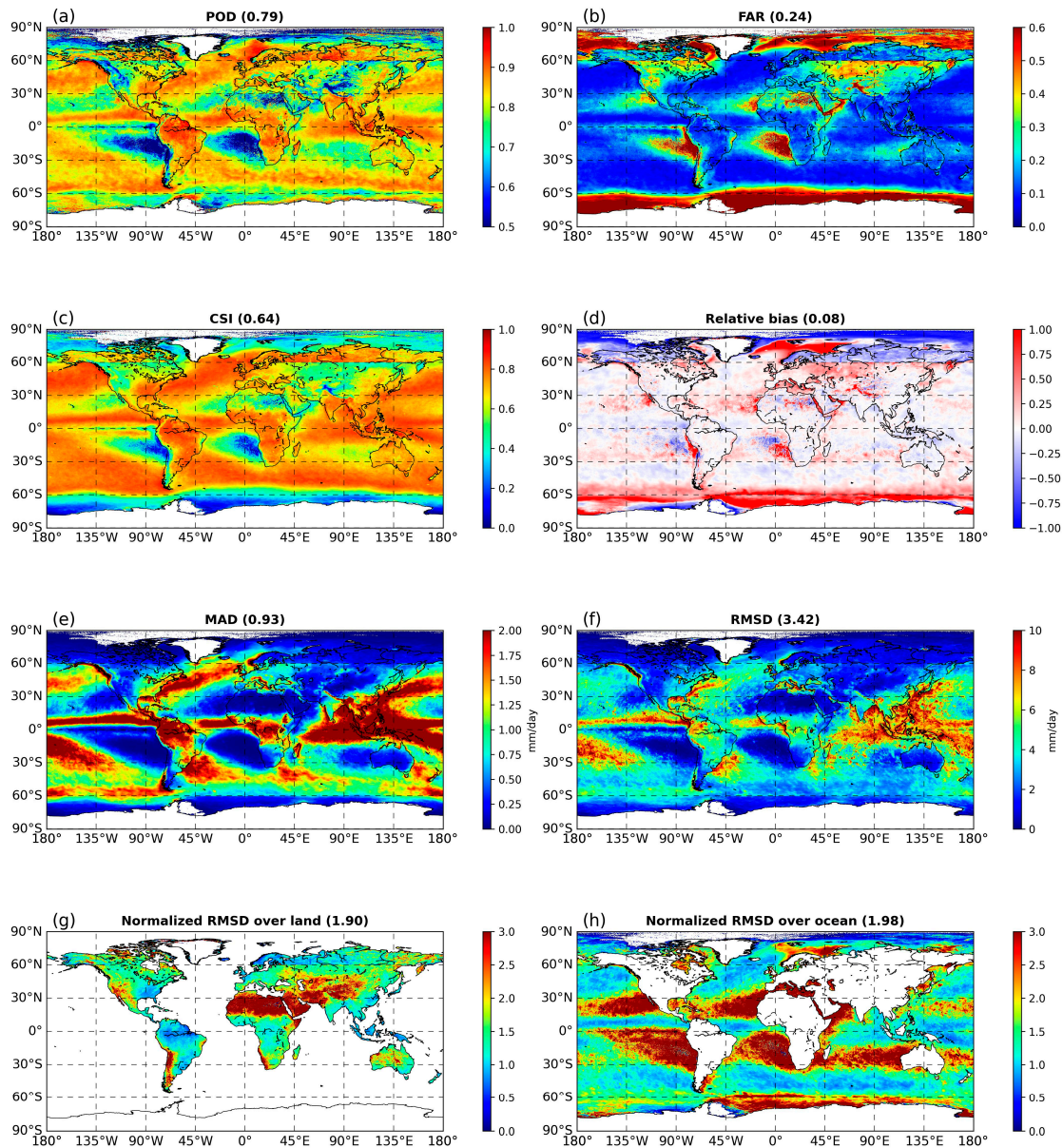


**Figure 4.** Maps of statistical description, POD (a), FAR (b), CSI (c), RB (d), MAD (e), RMSD (f), normalized RMSD over land (g), and normalized RMSD over ocean (h), of the differences between IMERG V06\_FR and V07\_FR.

As for the precipitation quantification metric, the global mean value of RB between V06\_FR and V07\_FR is less than 0.1 (Figure 4d). Within the latitudinal range of 60°N to 60°S, the average RB closely aligns with the global value, showing a deviation of only  $-2.4\%$  from the latter. What is more, IMERG V07\_FR in the 60°N-S band records a slightly reduced estimate of rainfall than IMERG V06\_FR, covering less than 40% of the total land and ocean area. The maximum RB (262.3) is located in North Greenland (81.35°N, 55.05°W) due to the much lower rainfall estimated here by IMERG V07\_FR. The local climate, topography condition, and the enhanced algorithm may jointly contribute to this estimation bias. The global mean MAD (0.93 mm/day) and RMSD (3.42 mm/day)

between these two versions is unignorable considering the daily mean precipitation value (2.19 and 2.12 mm/day for V06\_FR and V07\_FR, respectively) (Figure 4e,f). Especially, the MAD demonstrates significant variations in response to changes in precipitation (Figure 5). The global mean MAD increases from 0.59 to 9.3 mm/day as regions shift from daily precipitation levels between 1–2 to 20–40 mm/day. The MAD further shows a significant difference (0.16 vs. 2.17 mm/day,  $p < 0.01$ ) between dry (annual precipitation  $< 500$  mm) and wet regions (annual precipitation  $> 1500$  mm). Accordingly, the normalized RMSD is presented for land and ocean to eliminate the system bias reduced by precipitation amount. Results show that the normalized RMSD over land and ocean is similar in quantity (with the mean value being 1.90 for the land and 1.98 for the ocean), indicating a noticeable adjustment of V07\_FR. The aforementioned results indicate the capacity of IMERG V06\_FR and V07\_FR to quantify precipitation time series on a global scale. Thus, a more targeted assessment of IMERG's raw spatial resolution should be carried out within our research focus area, mainland China.

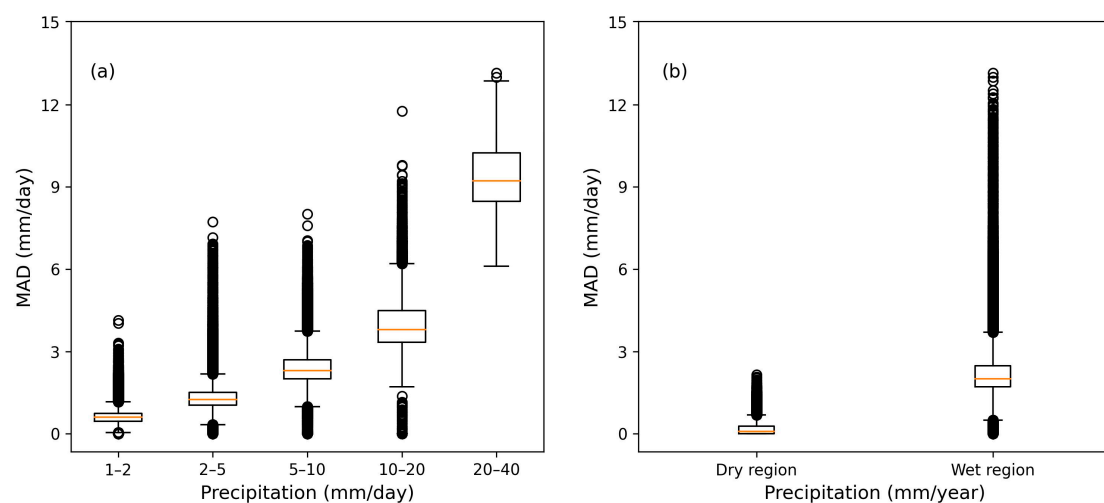


**Figure 5.** Boxplot of Means Absolute Difference (MAD) between IMERG V06\_FR and V07\_FR under ranges of different daily precipitation rates (a) and regions with different wetness (b).

### 3.2. Comparison of IMERG 06\_FR and 07\_FR in Mainland China

#### 3.2.1. Nation-Wide Evaluation

The performance of IMERG V06\_FR and V07\_FR is evaluated against the independent ground gauge observation (Figure 6) in precipitation estimation. The annual mean precipitation for IMERG V06\_FR and V07\_FR is 675.9 and 679.8 mm/year, respectively. This value is relatively higher than multi-year mean precipitation, i.e., 630 mm/year (China Climate Change Blue Book, 2022). National precipitation revealed by these two products exhibited similar spatial distribution features as compared with the gauge observation, i.e., higher precipitation in the southeast and lower precipitation in the northwest. The comparable spatial pattern indicates the capability of both IMERG V06\_FR and V07\_FR to capture precipitation characteristics. The IMERG V06\_FR and V07\_FR exhibit great spatial differences despite their comparable average values (Figure 6d). IMERG V07\_FR detects more precipitation than V06\_FR over 55.6% of grid cells across mainland China. Most of the differences larger than 100 mm/year are found in the southeast and southwest region while most of the negative variances are scattered in the Tibetan Plateau. Notably, the maxima of difference between IMERG V07\_FR and V06\_FR is 1915.9 mm/year (V06\_FR = 2027.5 mm/year and V07\_FR = 3943.39 mm/year), located near Nyingchi County, Tibet, China. The lack of local ground gauges, along with the correction bias, collectively contribute to this estimation bias.

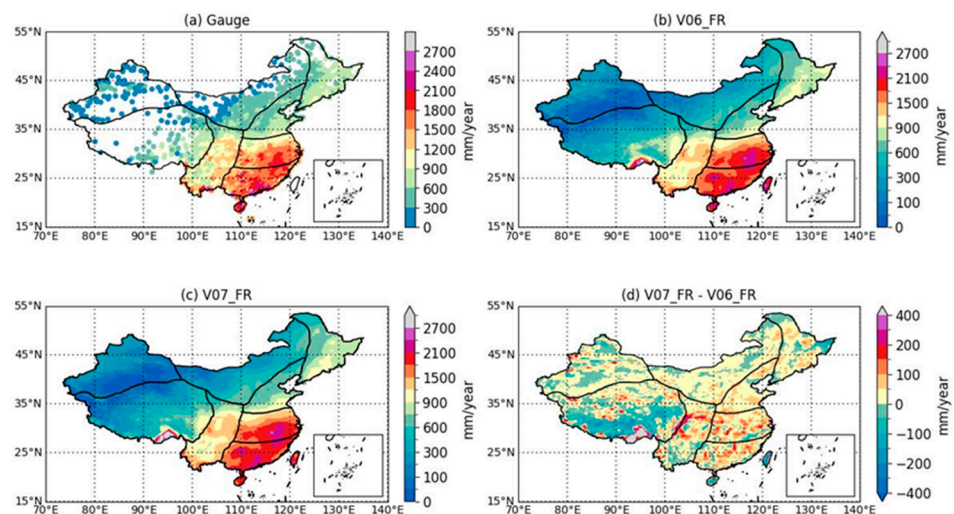


**Figure 6.** National-based evaluation of gauges (a), IMERG V06\_FR (b), V07\_FR (c), and differences between V07\_FR and V06\_FR (d) in annual mean precipitation estimation.

### 3.2.2. Grid-Based Evaluation

The selected IMERG products are further analyzed to evaluate their performance in estimating precipitation over mainland China. Notably, a direct comparison of gridded product and point-based product is subject to scale mismatches. The probability density functions (PDF) at a daily resolution for precipitation of the ground gauge and the two SPPs are presented in Figure 7. Ground gauge observations and the two IMERG FR products exhibit good consistence as for the precipitation distribution shape, reflecting IMERG's capability to reproduce precipitation of various categories. However, notable differences in precipitation detection exist when the daily precipitation rate falls below 5 mm/day. Both IMERG V06\_FR and V07\_FR within this range tend to detect more occurrences of precipitation than those of ground gauges: The satellite products both capture nearly 1.5 times and 1.3 times more of the precipitation occurrence than the ground gauge when precipitation ranges from 1 to 2 mm/day and from 2 to 5 mm/day, respectively. Nevertheless, the PDF shape of satellite products converges with gauge observations as the daily precipitation increases. The differences in PDF of different versions of IMERG products suggest that biases may exist where light rainfall tends to take place.

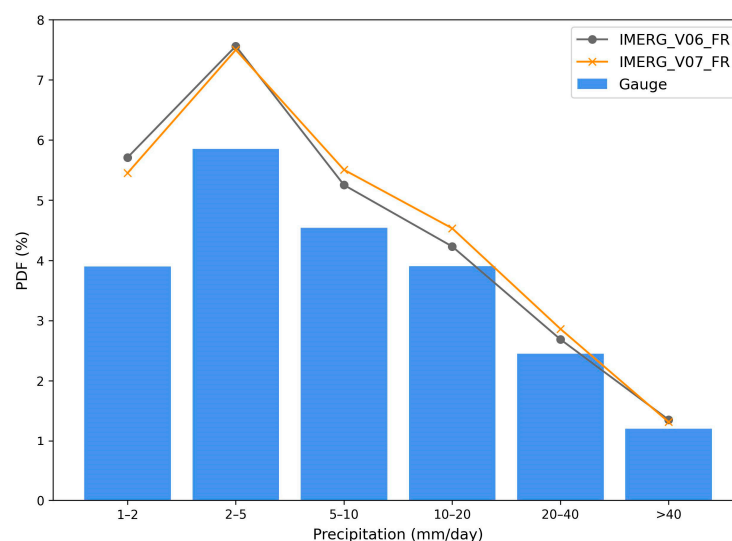


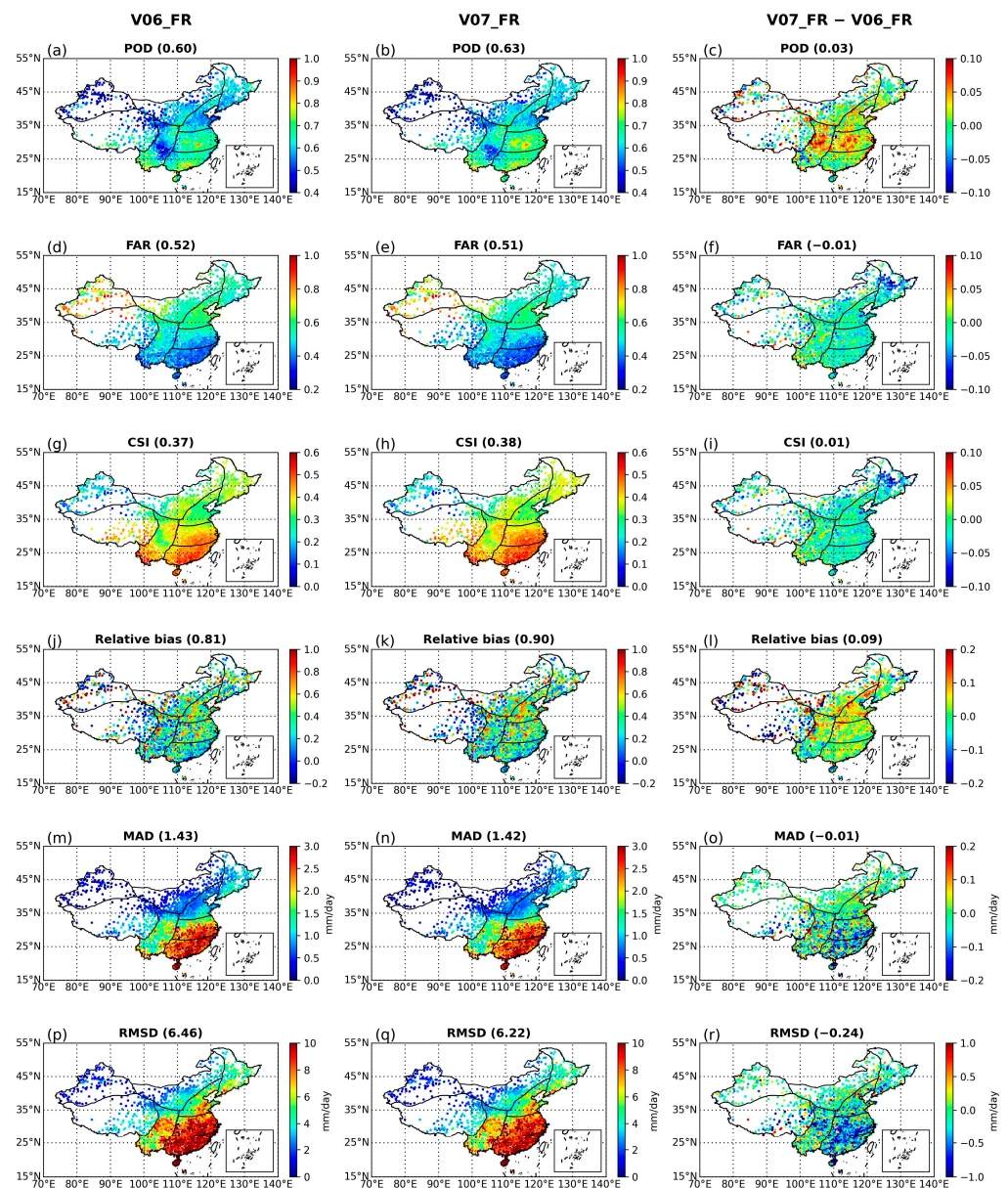
**Figure 7.** Probability density function (PDF) of gauge, IMERG V06\_FR, and IMERG V07\_FR of daily rainfall intensities from January 2016 to December 2020.

Gauge observation is selected as the benchmark product to calculate the statistical metrics of SPPs across mainland China. IMERG V07\_FR shows slight improvement compared with V06\_FR as for categorical indexes (Figure 8a–i). The POD increases by 5.0% as IMERG V07\_FR compared with its predecessor, with the enhancements mainly observed in Southern China. The two versions of SPPs not only share a close national mean FAR (Figure 8d,e), but they also exhibit a similar spatial distribution as revealed by their difference (Figure 8f). The CSI shows similar trends with FAR, indicating that IMERG V06\_FR and V07\_FR are of comparable capability in precipitation detection and accuracy over the target region. As for the quantitative measurement metrics, IMERG V07\_FR diverges more from the gauge values than V06\_FR, as indicated by the RB (0.90 vs. 0.81). What is more, the overestimation is mainly observed in the North China Plain and the Guanzhong Plain (Figure 8l). However, MAD and RMSD both reveal a reduction in error as the IMERG version transitions to V07\_FR, exhibiting decreases of 1.4% and 3.7%, respectively, in comparison to V06\_FR. The estimation errors are primarily concentrated in the southeastern regions of China (Figure 8m,n,p,q), where relatively abundant precipitation is common. Simultaneously, a significant improvement in precipitation accuracy is also evident in the same region (Figure 8o,r). This phenomenon indicates that areas with high precipitation levels tend to exhibit not only elevated MAD and RMSD values but also enhancements in measurement accuracy as for IMERG V07\_FR.

### 3.3. Spatial–Temporal Comparison of IMERG V06\_FR and V07\_FR across Mainland China

The two SPPs (IMERG V06\_FR and V07\_FR) both exhibit different performance under the eight sub-regions divided by climate (Table 2). Concerning the categorical indices, it is noteworthy that, irrespective of the product version, only three out of eight regions display higher level of POD, FAR, and CSI in relation to the national averages, both located in the humid zone (S, C, and SW). Specifically, the CSI of region C surpasses the national mean CSI for both IMERG V06\_FR and V07\_FR, with increases of 13.5% and 15.8%, respectively. Similarly, region S also demonstrates a significantly higher CSI than the national value for both IMERG V06\_FR and V07\_FR, showing respective increments of 24.3% and 26.3%. As for region SW, the CSI exhibits an identical level with the national average for V06\_FR and a slight improvement for V07\_FR (+2.6%). On the contrary, sub-regions with lower levels of categorical indices predominantly lie within the arid regions (WAS and EA) and the transitional zone (NE, N, and QT). The WAS region has the lowest CSI regardless of the IMERG version, with values less than 50% of the national average. Despite the regional difference, IMERG V07\_FR generally shows improvement across the eight sub-regions than IMERG V06\_FR in precipitation detection accuracy.

As for the quantitative results, region N exhibits the highest RB (>5.0), which is followed by EA (>1.8). What is more, the RB of region N and EA increases by 7.8% and 10.5% as IMERG V07\_FR compared with V06\_FR, respectively. The high density of ground gauges, particularly in areas proximate to region EA, combined with specific environmental and climatic conditions, may contribute to the elevated R observed in Region N. Other regions show relatively low RB (<1.0), and the differences between IMERG V07\_FR and V06\_FR vary across different regions. The QT region shows the most negative relative difference (−25.0%), while region C turns out to have the most positive difference (7.5%). The regional differences can be attributed to the joint effect of local topography and climate conditions. Different from RB, the MAD and RMSD values tend to be smaller for IMERG V07\_FR than IMERG V06\_FR (−6.7–0.0% for MAD and −11.1–0.0% for RMSD, respectively). The quantitative measure results indicate that IMERG V07\_FR can estimate precipitation more accurately across mainland China than V06\_FR.

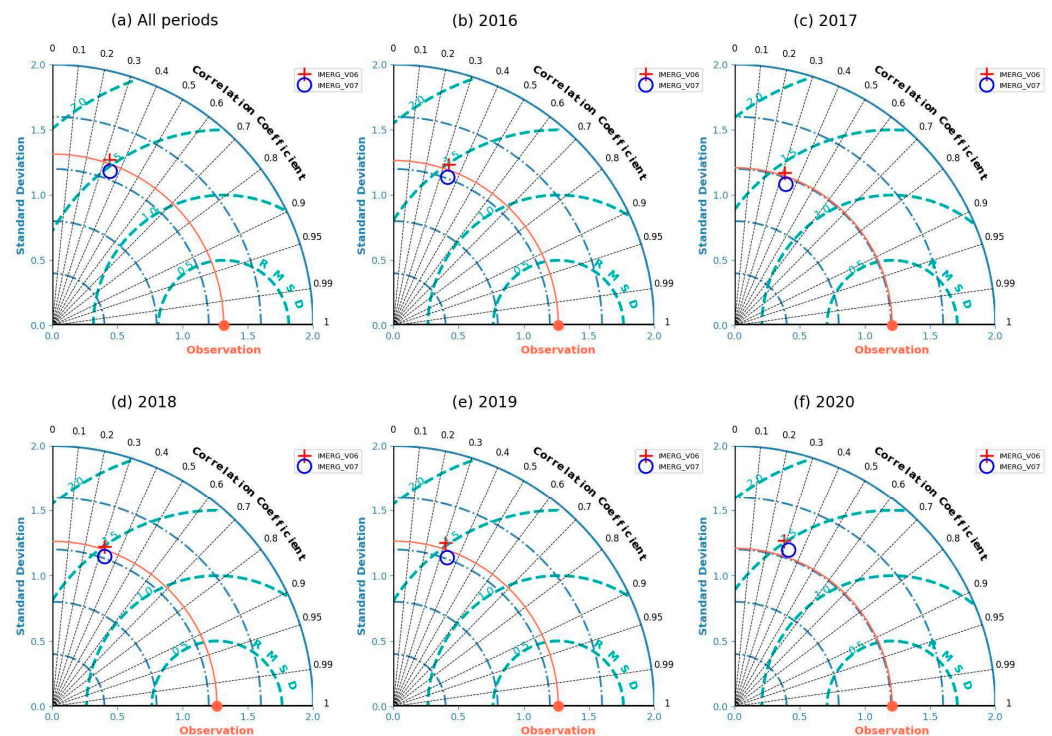


**Figure 8.** Spatial distribution of statistical metrics of IMERG V06\_FR (a,d,g,j,m,p), IMERG V07\_FR (b,e,h,k,n,q), and their differences (c,f,i,l,o,r).

The temporal comparison between the selected SPPs is investigated using the Taylor diagrams (Figure 9) in terms of CC, SD, and RMSD. The SD of gauge observations varies across the investigated years due to distinctive hydroclimatic features. However, the SD of IMERG V07\_FR generally exhibits a lower level than that of V06\_FR despite the hydrological year. This result suggests that the precipitation estimated by V07\_FR is of less variability across mainland China. The CC and RMSD of V07\_FR also exhibit a more reduced magnitude than V06\_FR regardless of hydrological years. These results further suggest that IMERG V07\_FR is more reliable than V06\_FR as for precipitation estimation. There is no evident distinction between hydrological years as for the temporal results revealed by Taylor diagram. This phenomenon indicates that the IMERG products exhibit a relatively stable performance across different hydrological years within the study period.

**Table 2.** Summary of daily statistical metrics for IMERG V06\_FR and V07\_FR across all monitored grid cells of mainland China from January 2016 to December 2020.

Region	Product	POD	FAR	CSI	RB	MAD mm/day	RMSD mm/day
WAS	V06_FR	0.41	0.73	0.18	0.90	0.029	0.096
	V07_FR	0.42	0.72	0.19	0.89	0.028	0.091
QT	V06_FR	0.57	0.50	0.36	0.36	0.10	0.27
	V07_FR	0.57	0.50	0.36	0.27	0.095	0.24
EA	V06_FR	0.58	0.58	0.32	1.9	0.16	0.58
	V07_FR	0.59	0.56	0.34	2.1	0.16	0.56
NE	V06_FR	0.60	0.55	0.34	0.38	0.15	0.47
	V07_FR	0.60	0.52	0.37	0.36	0.14	0.45
N	V06_FR	0.59	0.60	0.31	5.1	0.34	1.3
	V07_FR	0.61	0.58	0.33	5.5	0.33	1.3
C	V06_FR	0.66	0.47	0.42	0.40	0.70	1.9
	V07_FR	0.70	0.46	0.44	0.43	0.67	1.8
SW	V06_FR	0.59	0.49	0.37	0.36	0.56	1.6
	V07_FR	0.62	0.49	0.39	0.38	0.54	1.5
S	V06_FR	0.67	0.40	0.46	0.29	0.66	1.8
	V07_FR	0.68	0.38	0.48	0.30	0.63	1.7

**Figure 9.** Taylor diagrams consisting of correlation coefficient, normalized standard deviation, and normalized RMSD for daily precipitation estimates from IMERG V06\_FR and V07\_FR during all periods (a) and distinct hydrological years (b–f) over mainland China.

### 3.4. Comparison of IMERG V06\_FR and V07\_FR under Extreme Precipitation

The disparities between IMERG V06\_FR and V07\_FR under the scenario of extreme precipitation (>50 mm/day) are displayed in Figure 10. The annual extreme precipitation for V06\_FR and V07\_FR is 75.6 and 72.2 mm/year, respectively. What is more, the national average values of POD, FAR, and CSI are comparable for these two post-real-time SPPs, with only slight improvement observed in V07\_FR. However, variations in the accuracy of precipitation between them become evident when assessed at the grid level (Figure 10c,f,i). Especially the decreases in CSI are mainly observed in the region C (−0.04) and S (−0.02), which are prone to typhoon events. This phenomenon indicates that the adjustments of IMERG V07\_FR may lower the detection accuracy of precipitation along the southeast coastal area. In terms of continuous quantitative metrics, IMERG V07\_FR demonstrates enhanced accuracy in estimating extreme precipitation compared with V06\_FR, resulting in a 24.3% reduction in RB and a 2.3% decrease in RMSD.

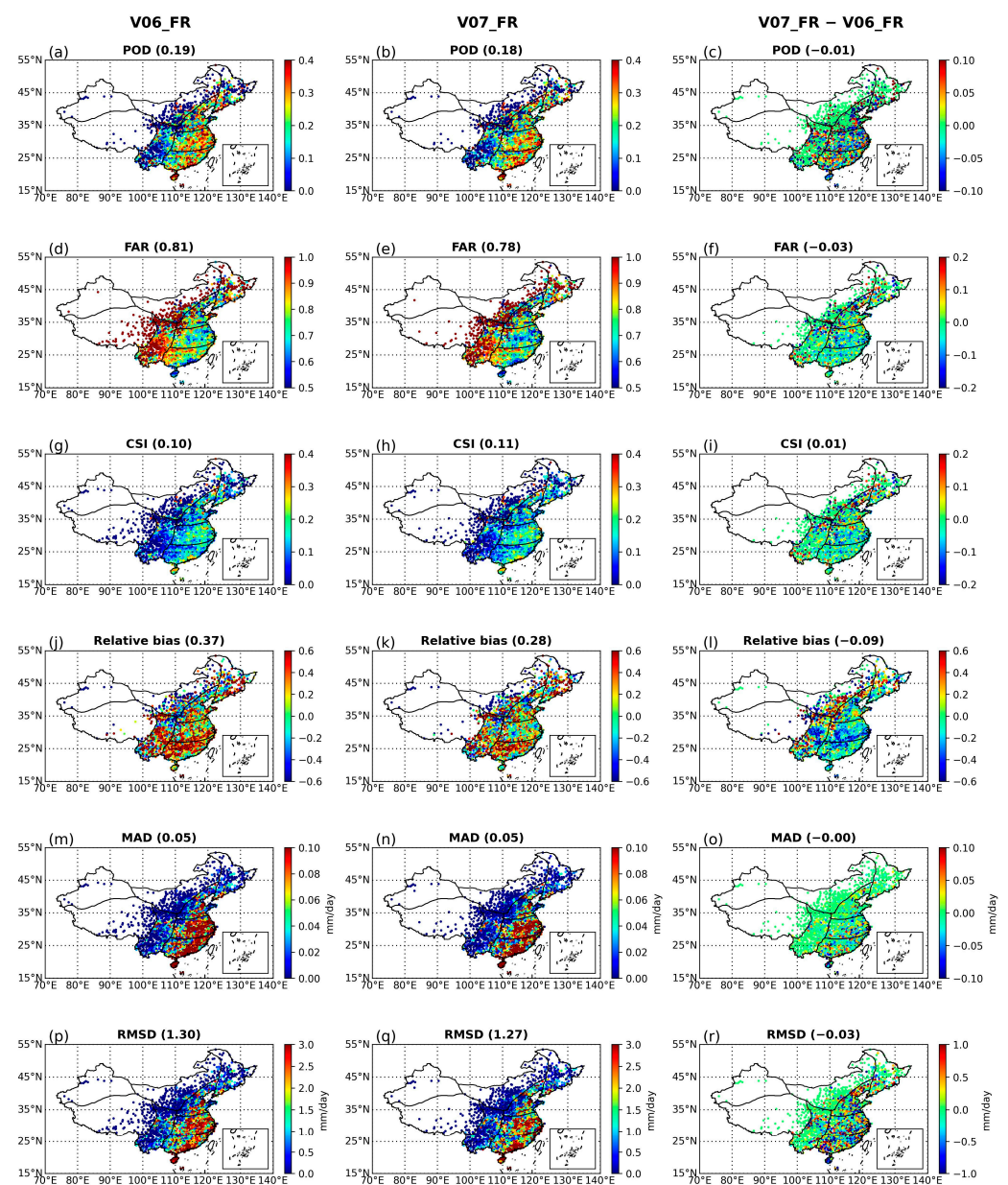


**Figure 10.** Spatial distribution of statistical metrics for IMERG V06 FR (a,d,g,j,m,p), IMERG V07 FR (b,e,h,k,n,q), and their differences (c,f,i,l,o,r) under extreme precipitation rate.

Table 3 further lists the performance of IMERG V06\_FR and V07\_FR during typical typhoon events in mainland China. IMERG V07\_FR shows stronger capability in both accurately capturing and estimating precipitation during typhoon events than IMERG V06\_FR. As for the precipitation detection metrics, the CSI values of IMERG V07\_FR are higher than the corresponding values of V06\_FR. This phenomenon is strengthened especially during typhoon events KHANUN (+25.4%), which is mainly due to the relatively short duration of this typhoon's landfall. The quantitative error measurement metrics show that the IMERG V07\_FR has lower MAD and RMSD values than V06\_FR for most of the typhoon events, except the HAITANG. The relatively higher error metrics of the event HAITANG can be attributed to its short duration (<1 day) in the current area of research interest. The better performance of IMERG V07\_FR for precipitation estimation under extreme precipitation rates and during typhoon events indicates its capability over IMERG V06\_FR in risk analysis.

**Table 3.** Statistical evaluation of IMERG V06\_FR and V07\_FR performance during typical typhoon events along the southeast coastline of mainland China.

Event Name	Start Date	End Date	Maximum Rainfall Amount (mm/day)	Product	POD	FAR	CSI	RB	MAD (mm/day)	RMSD (mm/day)
MERANTI	2016/9/9	2016/9/10	12,835.9	V06_FR	0.34	0.64	0.24	0.45	1.87	3.04
				V07_FR	0.33	0.64	0.24	0.35	1.73	2.83
HAIMA	2016/10/14	2016/10/15	7743.6	V06_FR	0.34	0.70	0.19	0.70	1.42	2.46
				V07_FR	0.36	0.63	0.23	0.54	1.38	2.34
MERBOK	2017/6/10	2017/6/11	9316.1	V06_FR	0.31	0.52	0.24	1.58	1.51	2.23
				V07_FR	0.39	0.45	0.31	1.29	1.40	2.03
HAITANG	2017/7/27	2017/7/28	6953.6	V06_FR	0.25	0.44	0.19	0.73	0.97	1.69
				V07_FR	0.31	0.55	0.21	1.24	1.04	1.79
KHANUN	2017/10/11	2017/10/12	6320.6	V06_FR	0.26	0.80	0.13	0.59	1.15	1.90
				V07_FR	0.22	0.80	0.12	0.84	1.15	1.87

## 4. Discussion

### 4.1. Similarities and Differences between IMERG V06\_FR and V07\_FR

Generally, the newly released IMERG V07\_FR shows a stronger capability of precipitation estimation than its predecessor V06\_FR. V07\_FR exhibits similarities as well as differences in comparison to V06\_FR across scales. Specifically, these two post-real-time SPPs show similar peak precipitation locations and error distributions. However, their differences become evident when examined at finer grid cell resolutions, such as regions where V07\_FR successfully detects precipitation that remains undetected by V06\_FR. The similarities can be attributed to the fact that the FR product is calibrated by the same precipitation ground reference product, i.e., the GPCC [15]. From a technical standpoint, the disparities in precipitation estimates between different SPP versions can be attributed to two distinct perspectives, i.e., the instruments and the algorithm. The IMERG sensors usually consist of a spaceborne radar, PMW imagers and sounders, and geosynchronous IR imagers [33]. The update and replacement of monitoring sensors naturally induce alterations in the estimated precipitation by SPPs. However, since the sensor updates for IMERG V07 were scheduled to commence in December 2021, the investigated period in the present study is not influenced. Therefore, it is reasonable to infer that variations in estimation and the changing error characteristics of precipitation datasets are primarily attributed to algorithm upgrades. For example, the enhancements in GPROF MW facilitate the detection of warm snowfall events, and the geolocation shift is corrected as well [28].

The advantages of GPROF V07 over its predecessors were also validated in the Netherlands by Bogerd et al. [38]. Moreover, there are long-lasting system errors that may cause differences among versions, such as the errors brought by snow, ice, uneven topography, and complex terrain in precipitation retrieval [39]. The upgraded algorithm, along with the uncertainties in monitoring precipitation in regions with certain climatic features and topography, jointly contribute to the distinctions among versions. These differences manifest in various ways, such as spatial variations in estimated precipitation and deviations in evaluation metrics when comparing the two IMERG versions. In future research, it is worthwhile to explore the quantified relationship between potential influencing factors and precipitation estimation errors.

#### 4.2. Varying Performance of IMERG in Different Climatic Regions

The performance of precipitation estimation by IMERG V07 varies under different sub-regions divided by climate features. The changing performance of IMERG products under various basins or climatic regions across mainland China has also been verified by Wang et al. [14] and Yu et al. [18]. Generally, warm and wet sub-regions tend to have lower RB and more accurate detection probability, while dry and high-elevation regions have higher RB and lower detection capability. The differences in precipitation detection and accuracy of quantification can be attributed to a combination of climatic conditions, elevation, and orography [40,41]. It is notable that the sub-region consisting of the northwestern region of China tends to have the lowest CSI. The local arid climate and sparse ground gauge observations jointly contribute to this phenomenon [42].

Furthermore, the IMERG products can consistently witness the maximum precipitation in China (the Yarlung Tsangpo Basin, located in the Southern Tibet region) since the start of the GPM era [14], while great uncertainties in estimation still exist, as indicated by variations between IMERG versions. The uncertainties in precipitation estimation also apply to regions with similar climate and topographic conditions [43]. The relatively high elevation of this region can also explain the uncertainty of precipitation estimation in the Tibet region [18]. Despite the regional differences, the performance of IMERG V07\_FR is superior to V06\_FR across mainland China, with higher CSI and lower RMSE. The refined KF to approximately preserve the local histogram of precipitation rates in V07\_FR may further explain the reduced error by the newly released SPPs [28].

#### 4.3. Study Limitations

The present study comparing V06\_FR with V07\_FR acknowledges several limitations, mainly when it comes to evaluation against ground gauges. Firstly, the density of gauges is recognized as a factor influencing the evaluation metrics. The number of ground gauges over mainland China in the present study is comparable to previous studies [39,44] and significantly larger than those utilized by Jiang et al. [45] and Yu et al. [18]. A higher gauge density is anticipated to yield improved performance for IMERG FR, particularly in continuous metrics, owing to its calibration against ground precipitation products [15]. The influence of gauge density may further manifest in sub-regions divided by climate. For instance, regions QT and WAS, characterized by sparse gauge density in the present dataset, may exhibit larger uncertainties compared to southern regions of China with denser ground gauges. Additionally, the spatial distribution of ground gauges introduces potential uncertainties in evaluating SPPs. In this study, metrics are computed for grid cells with at least one gauge, consistent with the criteria of Tang et al. [46]. However, this approach results in an uneven gauge number per pixel, introducing potential errors due to inherent differences in precipitation estimation between point-scale measurements by gauges and areal estimation by satellites [41]. Furthermore, the use of data spanning only five years in the current investigation raises considerations. Given the warming climate and potential shifts in precipitation trends, this duration may not adequately represent performance compared to a longer period or the full lifespan of data availability.

## 5. Conclusions

In the present study, the latest IMERG V07 final run product is first compared with its predecessor IMERG V06 final run at the global scale, and these two SPPs are further evaluated against the ground gauge over mainland China to assess their performance in detecting precipitation under different rates. The main conclusions of this study are as follows:

(1) The IMERG V07\_FR exhibits a slightly lower global annual mean precipitation compared to V06\_FR, while the V07\_FR tends to detect greater precipitation in regions with maxima annual precipitation no matter over land, oceans, or at the global scale. The MAD is unignorable when comparing V06\_FR with V07\_FR, accounting for nearly half of the estimated daily precipitation. The regions mainly affected by the revised algorithm of V07\_FR include North Africa, West Asia, and the oceans along the coastline of West Americas, West Africa, and West Oceania, as indicated by the normalized RMSD.

(2) As for the national scale, the estimated precipitation over mainland China by V07\_FR is comparable with that by V06\_FR. However, the spatial variation exhibits an uneven pattern. Compared to V06\_FR, V07\_FR tends to overestimate in regions along the southeastern coastal areas and underestimate primarily within the QT region.

(3) As for the grid scale, V07\_FR exhibits improved capability over V06\_FR in both precipitation detection and its accuracy when using the ground gauge as reference and this phenomenon gets strengthened when investigated at sub-regions divided by climate. However, the performance of V07\_FR exhibits spatial heterogeneity, with its estimation accuracy generally decreasing from the southeast region to the northwest region.

(4) IMERG V07\_FR further shows a stronger ability to detect extreme rainfall rates, and the performance varies by specific typhoon events. However, the uncertainty of V07\_FR in detecting storms still exists, as indicated by the uneven spatial distribution of its difference with V06\_FR in POD and RB.

In summary, IMERG V07\_FR exhibits significant differences in precipitation estimation as compared with V06\_FR across scales. Future investigations should focus on conducting comprehensive analyses of IMERG V07\_FR's performance, including extended temporal coverage and more extensive ground gauge validation. Furthermore, there is an urgent need to enhance the algorithms used for precipitation estimation over mainland China to further advance the accuracy and reliability of precipitation estimation.

**Author Contributions:** Conceptualization, Y.W. and Z.L.; methodology, Y.W. and Z.L.; software, Y.W.; validation, Y.W., Z.L. and L.G.; formal analysis, Y.W.; investigation, Y.W.; resources, Y.W., Z.L. and L.G.; data curation, Y.W., L.G. and Y.Z.; writing—original draft preparation, Y.W.; writing—review and editing, Z.L.; visualization, Y.W.; supervision, L.G. and X.P.; project administration, L.G. and X.P.; funding acquisition, L.G. and X.P. All authors have read and agreed to the published version of the manuscript.

**Funding:** This work was funded by the National Natural Science Foundation of China (42077012, 41771263 & 41571130053) and Jिंगgang Shan Agricultural Hi-tech District Project (20222-051261-1).

**Data Availability Statement:** The URLs for downloading the satellite precipitation data are contained within the article. The gauge data in this study are available on request from the corresponding author.

**Acknowledgments:** This work was supported by the National Natural Science Foundation of China (42077012, 41771263 & 41571130053) and Jिंगgang Shan Agricultural Hi-tech District Project (20222-051261-1). Special thanks go to the China Meteorological Administration for providing the ground-based precipitation data and the NASA science team for their efforts in providing accessibility to IMERG precipitation data.

**Conflicts of Interest:** The authors declare no conflict of interest.

## References

1. Ham, Y.G.; Kim, J.H.; Min, S.K.; Kim, D.; Li, T.; Timmermann, A.; Stuecker, M.F. Anthropogenic fingerprints in daily precipitation revealed by deep learning. *Nature* **2023**, *622*, 301–307. [[CrossRef](#)] [[PubMed](#)]
2. Hong, Y.; Adler, R.F.; Negri, A.; Huffman, G.J. Flood and landslide applications of near real-time satellite rainfall products. *Nat. Hazards* **2007**, *43*, 285–294. [[CrossRef](#)]
3. Maggioni, V.; Meyers, P.C.; Robinson, M.D. A review of merged high-resolution satellite precipitation product accuracy during the Tropical Rainfall Measuring Mission (TRMM) era. *J. Hydrometeorol.* **2016**, *17*, 1101–1117. [[CrossRef](#)]
4. Chen, M.; Nabih, S.; Brauer, N.S.; Gao, S.; Gourley, J.J.; Hong, Z.; Kolar, R.L.; Hong, Y. Can Remote Sensing Technologies Capture the Extreme Precipitation Event and Its Cascading Hydrological Response? A Case Study of Hurricane Harvey Using EF5 Modeling Framework. *Remote Sens.* **2020**, *12*, 445. [[CrossRef](#)]
5. Li, Z.; Chen, M.; Gao, S.; Hong, Z.; Tang, G.; Wen, Y.; Gourley, J.J.; Hong, Y. Cross-Examination of Similarity, Difference and Deficiency of Gauge, Radar and Satellite Precipitation Measuring Uncertainties for Extreme Events Using Conventional Metrics and Multiplicative Triple Collocation. *Remote Sens.* **2020**, *12*, 1258. [[CrossRef](#)]
6. Yong, B.; Liu, D.; Gourley, J.J.; Tian, Y.; Huffman, G.J.; Ren, L.; Hong, Y. Global view of real-time TRMM multisatellite precipitation analysis: Implications for its successor global precipitation measurement mission. *Bull. Am. Meteorol. Soc.* **2015**, *96*, 283–296. [[CrossRef](#)]
7. Ruhi, A.; Messenger, M.L.; Olden, J.D. Tracking the pulse of the Earth's fresh waters. *Nat. Sustain.* **2018**, *1*, 198–203. [[CrossRef](#)]
8. Papalexiou, S.M.; Montanari, A. Global and regional increase of precipitation extremes under global warming. *Water Resour. Res.* **2019**, *55*, 4901–4914. [[CrossRef](#)]
9. Skofronick-Jackson, G.; Petersen, W.A.; Berg, W.; Kidd, C.; Stocker, E.F.; Kirschbaum, D.B.; Kalar, R.; Braun, S.A.; Huffman, G.T.; Iguchi, T.; et al. The Global Precipitation Measurement (Gpm) Mission for Science and Society. *Bull. Am. Meteorol. Soc.* **2017**, *98*, 1679–1695. [[CrossRef](#)]
10. Huffman, G.J.; Bolvin, D.T.; Nelkin, E.J.; Wolff, D.B.; Adler, R.F.; Gu, G.; Hong, Y.; Bowman, K.P.; Stocker, E.F. The TRMM multisatellite precipitation analysis (TMPA): Quasi-global, multiyear, combined-sensor precipitation estimates at fine scales. *J. Hydrometeorol.* **2007**, *8*, 38–55. [[CrossRef](#)]
11. Funk, C.; Peterson, P.; Landsfeld, M.; Pedreros, D.; Verdin, J.; Shukla, S.; Husak, G.; Rowland, J.; Harrison, L.; Hoell, A.; et al. The climate hazards infrared precipitation with stations—A new environmental record for monitoring extremes. *Sci. Data* **2015**, *2*, 150066. [[CrossRef](#)] [[PubMed](#)]
12. Beck, H.E.; Dijk, A.V.; Levizzani, V.; Schellekens, J.; Miralles, D.G. MSWEP: 3-hourly 0.25° global gridded precipitation (1979–2015) by merging gauge, satellite, and reanalysis data. *Hydrol. Earth Syst. Sci.* **2017**, *2017*, 589–615. [[CrossRef](#)]
13. Huffman, G.J.; Bolvin, D.T.; Braithwaite, D.; Hsu, K.; Joyce, R.; Xie, P. Integrated multi-satellite retrievals for GPM (IMERG). *Precip. Meas. Mission. Tech. Doc.* **2014**, *1*, 343–353.
14. Wang, C.; Tang, G.; Han, Z.; Guo, X.; Hong, Y. Global intercomparison and regional evaluation of GPM IMERG Version-03, Version-04 and its latest Version-05 precipitation products: Similarity, difference and improvements. *J. Hydrol.* **2018**, *564*, 342–356. [[CrossRef](#)]
15. Li, Z.; Tang, G.; Hong, Z.; Chen, M.; Gao, S.; Kirstetter, P.; Gourley, J.J.; Wen, Y.; Yami, T.; Nabih, S.; et al. Two-decades of GPM IMERG early and final run products intercomparison: Similarity and difference in climatology, rates, and extremes. *J. Hydrol.* **2021**, *594*, 125975. [[CrossRef](#)]
16. Hamza, A.; Anjum, M.N.; Masud Cheema, M.J.; Chen, X.; Afzal, A.; Azam, M.; Shafi, M.K.; Gulakhmadov, A. Assessment of IMERG-V06, TRMM-3B42V7, SM2RAIN-ASCAT, and PERSIANN-CDR precipitation products over the Hindu Kush Mountains of Pakistan, South Asia. *Remote Sens.* **2020**, *12*, 3871. [[CrossRef](#)]
17. Moazami, S.; Najafi, M.R. A comprehensive evaluation of GPM-IMERG V06 and MRMS with hourly ground-based precipitation observations across Canada. *J. Hydrol.* **2021**, *594*, 125929. [[CrossRef](#)]
18. Yu, L.; Leng, G.; Python, A.; Peng, J. A comprehensive evaluation of latest GPM IMERG V06 early, late and final precipitation products across China. *Remote Sens.* **2021**, *13*, 1208. [[CrossRef](#)]
19. Li, X.; Sungmin, O.; Wang, N.; Huang, Y. Evaluation of the GPM IMERG V06 products for light rain over Mainland China. *Atmos. Res.* **2021**, *253*, 105510. [[CrossRef](#)]
20. Zhou, C.; Gao, W.; Hu, J.; Du, L.; Du, L. Capability of imerg v6 early, late, and final precipitation products for monitoring extreme precipitation events. *Remote Sens.* **2021**, *13*, 689. [[CrossRef](#)]
21. Aksu, H.; Taflan, G.Y.; Yaldiz, S.G.; Akgül, M.A. Evaluation of IMERG for GPM satellite-based precipitation products for extreme precipitation indices over Turkiye. *Atmos. Res.* **2023**, *291*, 106826. [[CrossRef](#)]
22. Ang, R.; Kinouchi, T.; Zhao, W. Evaluation of daily gridded meteorological datasets for hydrological modeling in data-sparse basins of the largest lake in Southeast Asia. *J. Hydrol. Reg. Stud.* **2022**, *42*, 101135. [[CrossRef](#)]
23. Su, J.; Lü, H.; Zhu, Y.; Cui, Y.; Wang, X. Evaluating the hydrological utility of latest IMERG products over the Upper Huaihe River Basin, China. *Atmos. Res.* **2019**, *225*, 17–29. [[CrossRef](#)]
24. Zhang, L.; Xin, Z.; Zhang, C.; Song, C.; Zhou, H. Exploring the potential of satellite precipitation after bias correction in streamflow simulation in a semi-arid watershed in northeastern China. *J. Hydrol. Reg. Stud.* **2022**, *43*, 101192. [[CrossRef](#)]
25. Hu, M.; Ma, R.; Xiong, J.; Wang, M.; Cao, Z.; Xue, K. Eutrophication state in the Eastern China based on Landsat 35-year observations. *Remote Sens. Environ.* **2022**, *277*, 113057. [[CrossRef](#)]

26. Tan, J.; Huffman, G.J.; Bolvin, D.T.; Nelkin, E.J. IMERG V06: Changes to the morphing algorithm. *J. Atmos. Ocean. Technol.* **2019**, *36*, 2471–2482. [[CrossRef](#)]
27. Huffman, G.J.; Bolvin, D.T.; Nelkin, E.; Tan, J. On the Verge of IMERG Version 07. Presented at 2021 Fall Meeting, AGU, New Orleans, LA, USA, 13–17 December 2021.
28. Huffman, G.J.; Bolvin, D.T.; Joyce, R.; Nelkin, E.; Tan, J. *Lessons Learned in V07 IMERG*; UMBC Faculty Collection: Vienna, Austria, 2023.
29. Zhang, J.; Lin, Z. *Climate in China*; Shanghai Scientific and Technical Publishers: Shanghai, China, 1985. (In Chinese)
30. Xiao, M.; Zhang, Q.; Singh, V.P.; Chen, X. Regionalization-based spatiotemporal variations of precipitation regimes across China. *Theor. Appl. Climatol.* **2013**, *114*, 203–212. [[CrossRef](#)]
31. Sui, X.; Li, Z.; Ma, Z.; Xu, J.; Zhu, S.; Liu, H. Ground validation and error sources identification for GPM IMERG product over the southeast coastal regions of China. *Remote Sens.* **2020**, *12*, 4154. [[CrossRef](#)]
32. Shen, Z.; Zhang, Q.; Singh, V.P.; Sun, P.; He, C.; Cheng, C. Station-based non-linear regression downscaling approach: A new monthly precipitation downscaling technique. *Int. J. Climatol.* **2021**, *41*, 5879–5898. [[CrossRef](#)]
33. Huffman, G.J.; Bolvin, D.T.; Joyce, R.; Nelkin, E.J.; Tan, J.; Braithwaite, D.; Hsu, K.; Kelley, O.A.; Nguyen, P.; Sorooshian, S.; et al. NASA Global Precipitation Measurement (GPM) Integrated Multi-Satellite Retrievals for GPM (IMERG). Algorithm Theoretical Basis Document (ATBD) Version, 7. 2023. Available online: <https://gpm.nasa.gov/taxonomy/term/947> (accessed on 28 November 2023).
34. Huffman, G.J.; Bolvin, D.T.; Nelkin, E.J.; Stocker, E.F.; Tan, J. *V06 IMERG Release Notes*; NASA/GSFC: Greenbelt, MD, USA, 2020.
35. Catto, J.L.; Jakob, C.; Nicholls, N. Can the CMIP5 models represent winter frontal precipitation? *Geophys. Res. Lett.* **2015**, *42*, 8596–8604. [[CrossRef](#)]
36. Wei, G.; Lü, H.; Crow, W.T.; Zhu, Y.; Su, J.; Ren, L. Comprehensive evaluation and error-component analysis of four satellite-based precipitation estimates against gauged rainfall over Mainland China. *Adv. Meteorol.* **2022**, *2022*, 9070970. [[CrossRef](#)]
37. Taylor, K.E. Summarizing multiple aspects of model performance in a single diagram. *J. Geophys. Res. Atmos.* **2001**, *106*, 7183–7192. [[CrossRef](#)]
38. Bogerd, L.; Leijnse, H.; Overeem, A.; Uijlenhoet, R. Assessing sampling and retrieval errors of GPROF precipitation estimates over The Netherlands. *EGU Sphere* **2023**, *2023*, 1–22.
39. Tang, G.; Ma, Y.; Long, D.; Zhong, L.; Hong, Y. Evaluation of GPM Day-1 IMERG and TMPA Version-7 legacy products over Mainland China at multiple spatiotemporal scales. *J. Hydrol.* **2016**, *533*, 152–167. [[CrossRef](#)]
40. Dinku, T.; Ceccato, P.; Grover-Kopec, E.; Lemma, M.; Connor, S.J.; Ropelewski, C.F. Validation of satellite rainfall products over East Africa’s complex topography. *Int. J. Remote Sens.* **2007**, *28*, 1503–1526. [[CrossRef](#)]
41. Tang, G.; Long, D.; Hong, Y.; Gao, J.; Wan, W. Documentation of multifactorial relationships between precipitation and topography of the Tibetan Plateau using spaceborne precipitation radars. *Remote Sens. Environ.* **2018**, *208*, 82–96. [[CrossRef](#)]
42. Sharifi, E.; Steinacker, R.; Saghafian, B. Assessment of GPM-IMERG and other precipitation products against gauge data under different topographic and climatic conditions in Iran: Preliminary results. *Remote Sens.* **2016**, *8*, 135. [[CrossRef](#)]
43. Kumar, M.; Hodnebrog, Ø.; Daloz, A.S.; Sen, S.; Badiger, S.; Krishnaswamy, J. Measuring precipitation in Eastern Himalaya: Ground validation of eleven satellite, model and gauge interpolated gridded products. *J. Hydrol.* **2021**, *599*, 126252. [[CrossRef](#)]
44. Li, C.; Tang, G.; Hong, Y. Cross-evaluation of ground-based, multi-satellite and reanalysis precipitation products: Applicability of the Triple Collocation method across Mainland China. *J. Hydrol.* **2018**, *562*, 71–83. [[CrossRef](#)]
45. Jiang, L.; Bauer-Gottwein, P. How do GPM IMERG precipitation estimates perform as hydrological model forcing? Evaluation for 300 catchments across Mainland China. *J. Hydrol.* **2019**, *572*, 486–500. [[CrossRef](#)]
46. Tang, G.; Clark, M.P.; Papalexiou, S.M.; Ma, Z.; Hong, Y. Have satellite precipitation products improved over last two decades? A comprehensive comparison of GPM IMERG with nine satellite and reanalysis datasets. *Remote Sens. Environ.* **2020**, *240*, 111697. [[CrossRef](#)]

**Disclaimer/Publisher’s Note:** The statements, opinions and data contained in all publications are solely those of the individual author(s) and contributor(s) and not of MDPI and/or the editor(s). MDPI and/or the editor(s) disclaim responsibility for any injury to people or property resulting from any ideas, methods, instructions or products referred to in the content.